Materials Today Physics 14 (2020) 100219

Contents lists available at ScienceDirect

Materials Today Physics

journal homepage: https://www.journals.elsevier.com/materials-today-physics

Stretchable tactile sensor with high sensitivity and dynamic stability based on vertically aligned urchin-shaped nanoparticles

Z. Yu [a, b, c, g], W.B. Ying [d, g], D. Pravarthana [a, c], Y.Y. Li [a, c, f], G.Y. Mao [e], Y.W. Liu [a, b, c], C. Hu [a, b], W.X. Zhang [a, b, c], P.X. He [a, c, f], Z.C. Zhong [a, b, c], S.X. Qu [e], R.Y. Zhang [d, ***], J. Shang [a, b, c, **], J. Zhu [d], R.-W. Li [a, b, c, *]

[a] CAS Key Laboratory of Magnetic Materials and Devices, Ningbo Institute of Materials Technology and Engineering, Chinese Academy of Sciences, Ningbo 315201, PR China
[b] College of Materials Science and Opto-Electronic Technology, University of Chinese Academy of Sciences, Beijing 100049, PR China
[c] Zhejiang Province Key Laboratory of Magnetic Materials and Application Technology, Ningbo Institute of Materials Technology and Engineering, Chinese Academy of Sciences, Ningbo 315201, PR China
[d] Key Laboratory of Bio-based Polymeric Materials Technology and Application of Zhejiang Province, Ningbo Institute of Materials Technology and Engineering, Chinese Academy of Sciences, Ningbo 315201, PR China
[e] State Key Laboratory of Fluid Power and Mechatronic System, Key Laboratory of Soft Machines and Smart Devices of Zhejiang Province, Department of Engineering Mechanics, Zhejiang University, Hangzhou 310027, China
[f] College of Information Engineering, Nanjing University of Finance and Economics, Nanjing, 210046, China

ARTICLE INFO

Article history:
Received 14 February 2020
Received in revised form
24 March 2020
Accepted 5 April 2020
Available online 4 May 2020

Keywords:
Stretchable E-skin
Elastic modulus regulation
Urchin-shaped conductive magnetic nanoparticles
Pressure sensitivity
Stretching insesnitivity

ABSTRACT

Stretchable tactile sensor (STS) is promising for wearable electrical devices, human-machine interfaces, and electronic skin. However, developing a STS based on piezoresistive composite high-pressure sensitivity and dynamic stability remains challenging because stretching deformation destroys the original dispersed state of conductive fillers. This interference of stretching strain on the pressure sensing greatly reduces device performance. Here, we realize an STS based on a piezoresistive composite with different elastic modulus in its functional regions. The composite contains high elastic modulus region (59.1 MPa) of vertically aligned columns of urchin-shaped nanoparticles, and low elastic modulus region (2.4 MPa) of pure matrix. The sensor exhibits high-pressure sensitivity (12.05 kPa^{-1}) owing to the increased conductive contact area between urchin-shaped nanoparticles in the high elastic modulus region. While stretching to 400% strain, the sensor exhibits excellent dynamic stability via strain accommodation in the low elastic modulus region. Our design to separate sensing from multiple stimulus by elastic modulus regulation is easy operative and universal. In addition, the sensor has a low hysteresis coefficient (5.25%), a good detection limit (22 mg), a low response/recovery time (<50 ms), and an excellent mechanical durability (cycled 10,000 times). Finally, we demonstrate the use of our STS for several important stretchable electronic applications to show the feasibility of our design.

1. Introduction

In the past decades, the sensor development has rapidly shifted from traditional rigid sensor to flexible sensors [1–6]. To meet the requirements of new applications, next-generation stretchable and elastic sensors are required [7–11]. In particular, tactile sensors are an important front-end component for many electronic systems because of their high sensitivity to slight pressure (<1 kPa) [3–5,10–13]. Therefore, the development of a stretchable tactile sensor (STS) has attracted great attention [7–9,14–18], which may enable novel electronic systems, such as wearable electrical devices (WED) [19–21], human-machine interfaces (HMI) [17,22,23], and electronic skin (E-skin) [23–25].

Existing flexible tactile sensors commonly use piezoresistive, piezocapacitive, piezoelectric, or triboelectric mechanisms for converting the pressure sensing into electrical signals [12,26]. Piezoresistive composites made from a stretchable polymer matrix filled with randomly dispersed conductive fillers have high sensitivity and intrinsic stretchability [26–30]. The mechanism of

* Corresponding author.
** Corresponding author.
*** Corresponding author.
E-mail addresses: zhangruoy@nimte.ac.cn (R.Y. Zhang), shangjie@nimte.ac.cn (J. Shang), runweili@nimte.ac.cn (R.-W. Li).
[g] These authors contribute equally to this work.

https://doi.org/10.1016/j.mtphys.2020.100219
2542-5293/

pressure sensing is based on the piezoresistive effect [11,13,26], where the electrical resistance decreases with an increased pressure leading to a regular increase in the detection current. In conventional piezoresistive composites, stretching strain seriously inhibits pressure sensing to prevent it from being use in stretchable and elastic applications [14,15,31,32]. When stretched, the state of the dispersed conductive fillers changes, producing a significant pseudo-electrical response that interferes with pressure detection and leads to low dynamic stability [26,33]. Avoiding this interference from stretching strain is necessary to obtain high-performance STS materials made from piezoresistive composites.

In view of the top-down strategy, researchers have designed several piezoresistive composites with special microstructure to fabricate STS, which are only sensitive to pressure stimulus and maintain high sensitivity during stretching (i.e. dynamic stability) [14,15,31–36]. For example, the Choong et al. [14], Roh et al. [15], Wang et al. [31], and Chang et al. [32] have reported STSs using piezoresistive composites with micropyramid arrays, 3D bump-valley micropattern arrays, 3D hierarchically porous, and Shar-Pei-like hierarchical wrinkles structures, respectively. Their sensors exhibit good dynamic stability of pressure sensitivity ($0.1–10\ kPa^{-1}$) under stretching strains of 30–60% [14,15,31–35]. These microstructures mostly consist of concave-convex structures. The convex regions enable pressure sensing, whereas the concave regions release the stretching strain [15]. The stretching strain is locally concentrated in the concave region due to its small thickness, which reduces the interference effects on the pressure sensing convex regions. In other words, these microstructures avoid the interference through strain accommodation [33]. However, this top-down strategy of engineered design is ineffective for strain accommodation under large stretching deformation (>100% strain), which is required for human joints and soft robots [14,36,37]. In addition, these approaches require sophisticated micromachining techniques to fabricate the STSs [36]. Presently, some researchers have adopted the bottom-up strategy to fabricate flexible pressure sensors with high performance and low cost. For example, Lee et al. [24] used composite nanofibres of carbon nanotubes and graphene to fabricate a bending-insensitive pressure sensor. These fibers change their relative alignment to accommodate bending deformation, thus reducing the strain in individual fibers. Coincidentally, Chen et al. [38] and Lee et al. [39] have prepared pressure-insensitive strain sensor based on carbonized crepe paper with aligned cellulose fibers, and highly aligned carbon nanofiber films. Therefore, a bottom-up strategy with aligned functional fillers to regulate the stretching strain of the different functional regions in piezoresistive composite is an interesting alternative method to solve the existing challenges in STSs.

In this article, we report a piezoresistive composite with different elastic modulus in its functional regions. The composite is prepared by a simple magnetic field–controlled assembly of urchin-shaped conductive magnetic nanoparticles (US-CMNPs) that acts as filler in a polyurethane (PU) elastic matrix (Scheme 1a). The elastomer filled with US-CMNPs column and the pure matrix of PU are the functional regions for sensing the pressure and releasing the stretching strain, respectively. The elastic modulus difference between these regions will be large because US-CMNPs column region consists of rigid particles (high modulus) and stretchable PU (low modulus). When a pressure is loaded onto the composite, the conductive contact area density of US-CMNPs increases in its column region, which leads to a significant electrical response (Scheme 1b). When it is stretched, the deformation occurs in pure matrix region without impacting the structure in US-CMNPs column region to achieve strain accommodation at large stretching strain (i.e. retention of original conductive path), thereby keeping a high-pressure sensitivity of intact composite (Scheme 1b). Thus, the fabricated STS based on our piezoresistive composite exhibits high-pressure sensitivity ($12.05\ kPa^{-1}$) and good dynamic stability (400% strain), which is most outstanding in the reported STSs. The practical viability of our STS is tested by several prototype stretchable electronic systems, such as WED for detecting the touching on knee, HMI for controlling the balloon volume, and E-skin with 6×6 pixels array.

2. Results and discussion

2.1. Sensor production

In accordance with our design, the synthesis of US-CMNPs is critical to obtain STSs. The urchin-shape conductive filler enables large electrical response for piezoresistive composite, which has been confirmed by previous reports [27,30,40]. In addition, it can be self-assembled to form the dispersed state (vertical alignment and horizontal isolation) under the vertical magnetic field [41]. Here, we choose the chemical reduction method to synthesize US-CMNPs made from magnetic silver-nickel NP cores and shelled with gold nanoneedles, as shown in Fig. 1a. Briefly, Ni nanoparticles are coated with Ag by a silver mirror reaction (Ag-Ni nanoparticles). These seed particles are combined with the $HAuCl_4 \cdot 4H_2O$ solution, which provides Au^{3+}. Levodopa (L-Dopa) is then added to reduce Au^{3+} for the growth of the Au nanoneedle shell on the surface of the Ag-Ni nanoparticles. This shell is formed because of reduced Au atoms grow on oriented, low-energy crystal faces under the induction of L-Dopa [42,43]. Finally, the synthetic US-CMNPs are blended with a PU solution, and this mixture is dried at high temperature under a vertical magnetic field to align the US-CMNPs vertically, producing the desired piezoresistive composite (US-CMNPs@PU). A more detailed procedure of the composite synthesis can be found in the Experimental Section.

As shown in the Scanning Electron Microscope (SEM) image of Fig. 1b, the synthesized particles exhibit the desired urchin-shaped micromorphology, with an aspect ratio of 3:1 for the Au nanoneedle shells. From the cross-section SEM image of prepared US-CMNPs@PU (Fig. 1c), a vertical arrangement of US-CMNPs can be seen in the non-planar ring (NPR)-PU matrix, which occurs due to the self-assembly of magnetic particles induced by the external vertical magnetic field. This is also confirmed by the presence of vertical stripes of Au in the Energy Dispersive Spectrometer (EDS) mapping (Fig. 1c). On the top surface of US-CMNPs@PU (Fig. 1d), there are microprotrusions of US-CMNPs columns, which are separated from each other in the horizontal plane. The horizontal spacing can be better seen from optical microscope images. Nanoindentation was used to test the elastic modulus of the two different functional regions based on the load force generated by the pressing head displacement of 1,000 nm from the top surface. From the results (Fig. 1e), the elastic modulus of the US-CMNPs column region and pure matrix region are found to be 59.1 MPa and 2.4 MPa, respectively, a factor of 24.6 difference in elastic modulus between the two regions.

The anisotropic arrangement of conductive filler leads to a higher resistivity along the horizontal direction ($3.1 \times 10^{11}\ \Omega\ m$) compared to vertical ($8.3 \times 10^{4}\ \Omega\ m$). The dispersed filler structures are not affected by the stretchability of US-CMNPs@PU, as evidenced by large breaking elongation values equal to 636.83% strain. The US-CMNPs@PU sample also can be stretched to approximately 300% strain, even with a notch of 1 mm width.. Importantly, the relative resistance change ($\Delta R/R_0$) of our piezoresistive composite is only 3.7% under large stretching strain of 600%, as shown in Fig. 1f. Its gauge factor (GF) is 6.17×10^{-5}, which is nearly three orders of magnitude lower than other reports. The GF is defined as

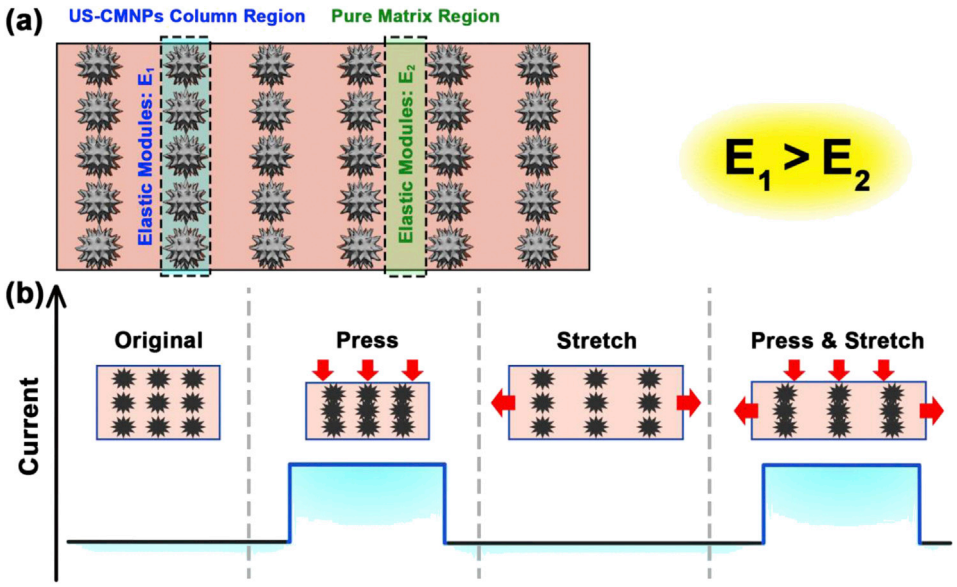

Scheme 1. (a) Schematic illustration of designed piezoresistive composite with different elastic modulus in its functional regions. (b) Expected electrical response curve of STS based on designed composite under different sensing states. STS, stretchable tactile sensor.

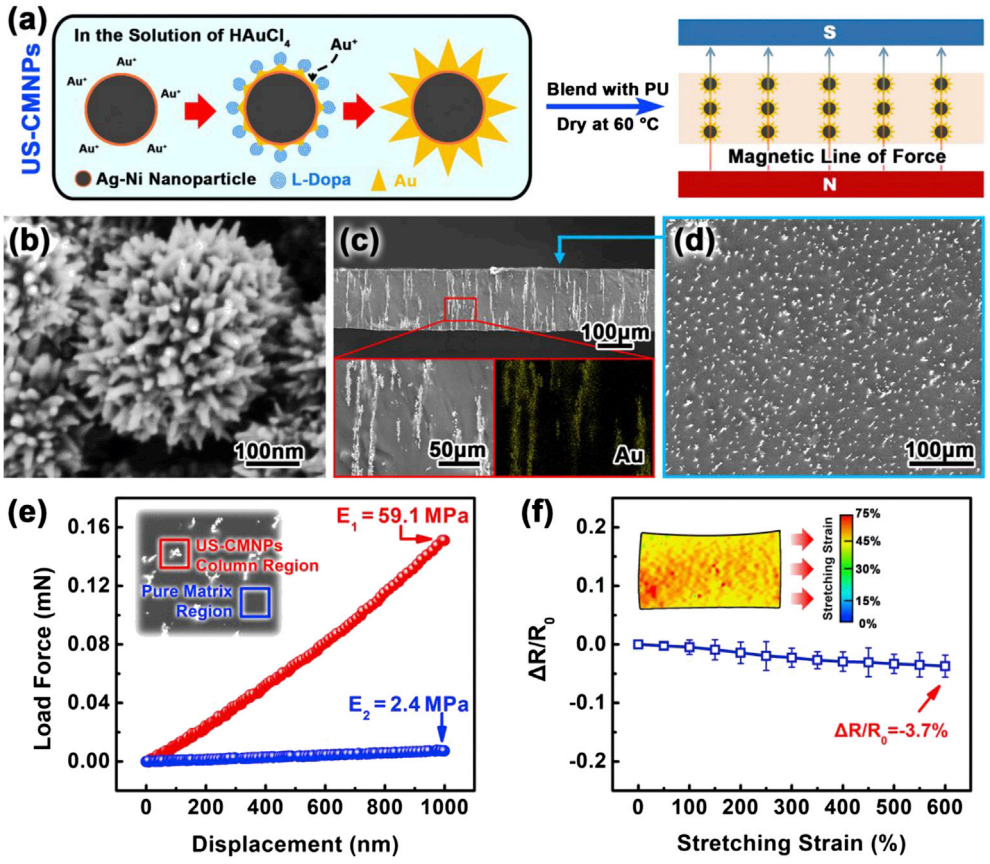

Fig. 1. (a) Schematic representation of synthesis steps involved for US-CMNPs, and US-CMNPs@PU composite. (b) SEM image of US-CMNPs. (c) SEM cross-sectional view images of US-CMNPs@PU composite along with its magnified region, and the corresponding EDS mapping of Au element. (d) SEM top view image of US-CMNPs@PU composite. (e) Force-displacement curves of nanoindentation at US-CMNPs column region (red) and pure matrix region (blue). Inset is SEM top view image of composite to show the testing region of nanoindentation. (f) Relative resistivity change of US-CMNPs@PU composite as a function of stretching strain. Inset is a color mapping of stretching strain distribution, when the sample is stretched to 75% strain. US-CMPNs, urchin-shaped conductive magnetic nanoparticles. PU, polyurethane, EDS, Energy Dispersive Spectrometer, SEM, Scanning Electron Microscope.

the ratio of $\Delta R/R_0$ induced by stretching. The low GF indicates the sensor is relatively insensitive to stretching strain. To understand the mechanism of deformation during stretching, the three-dimensional motion and deformation measurement system of ARAMIS (GOM, Germany) was used to image the in situ deformation under the stretching strain. From the results (inset of Fig. 1f), the large strain region (shown in red) displays regular streaks in the strain distribution color map. This indicates that the deformation mainly occurs in the matrix regions between the NP vertical columns when stretched horizontally, which suggests good strain accommodation in the composite.

To assemble the STS from US-CMNPs@PU, an elastic conductive electrode is required. Elastic electrodes based on a 3D-calabash bunch conductive network of liquid metals (LMs) are assembled as top and bottom conductive electrodes for the STS. The US-CMNPs@PU is located between the two elastic electrodes to form a sandwich structure. The LM-based elastic electrode used here is similar to our previous reports [44], but an additional protective layer of Ag NPs is introduced on the surface of the conducting layers to prevent LM leakage. The resistance of this elastic electrode is insensitive to the stretching strain ($\Delta R/R_0 = 0.69$ @ 400% stretching strain which prevents stretching interference form the electrodes of STS.

2.2. Device testing

First, the relative detection current change rate ($\Delta I/I_0$) as a function of pressure was measured to determine the pressure sensitivity of our STS, as shown in Fig. 2a. Here, I_0 is the initial current through the STS without loading, and ΔI is the current change under ΔP pressure loading. The sensitivity (S) of the STS is calculated using the following equation:

$$S = \frac{\Delta I/I_0}{\Delta P} \quad (1)$$

The sensitivity results (Fig. 2a) indicate that our STS exhibits a high sensitivity to pressure. The pressure sensitivity of the sensor is 12.05 kPa^{-1} with good linearity ($R^2 = 0.983$). Besides, we tested the sensitivity of six samples to verify the reproducibility of the sensor. Each sample was tested for five times and shows a similar pressure sensitivity from 11.94 kPa^{-1} to 12.16 kPa^{-1}. The high sensitivity can be attributed to the rough structure of the US-CMNPs and also from the microprotrusions of filler columns on the top surface of composite, which enables an increase in conductive contact area during pressure sensing. Previous studies show that microprotrusions on the surface of sensing material improve the detectivity at low pressure [18,45–50]. To validate this point, several US-CMNPs@NPR-PU samples with microprotrusions of different heights were prepared by applying different magnetic field intensities (500 Gs, 800 Gs, 1,200 Gs, 1,500 Gs). The surface roughness from topographies of these samples, which was tested by laser scanning confocal microscopy. The height of the microprotrusions increases with increased magnetic field intensity . The main peak of the micro-protrusion heights is 1.51 μm, 2.45 μm, 3.68 μm, and 5.16 μm, for the applied magnetic field of 500 Gs, 800 Gs, 1,200 Gs, and 1,500 Gs, respectively. The pressure response of piezoresistive sensors based on these samples was also tested, and the results. The sensitivity of these different sensors varies greatly from 3.09 kPa^{-1} to 12.05 kPa^{-1}. This variation demonstrates that both the microprotrusions on the surface and the piezoresistive effect of US-CMNPs@PU play a pronounced role in pressure sensitivity.

Further, we explored the stretching strain interference on the pressure sensitivity of the STS by comparing the $\Delta I/I_0$ vs. pressure curve at different stretching strains of 0, 200, and 400%. Fig. 2a shows that the electrical response of the STS to pressure remains essentially unchanged under various stretching strains. Even when stretched to higher strain, the pressure sensitivity still remains at a high level ($S = 11.29$ kPa^{-1} @ 200% strain, and $S = 10.84$ kPa^{-1} @ 400% strain). Moreover, the effect of repeated stretching cycles on

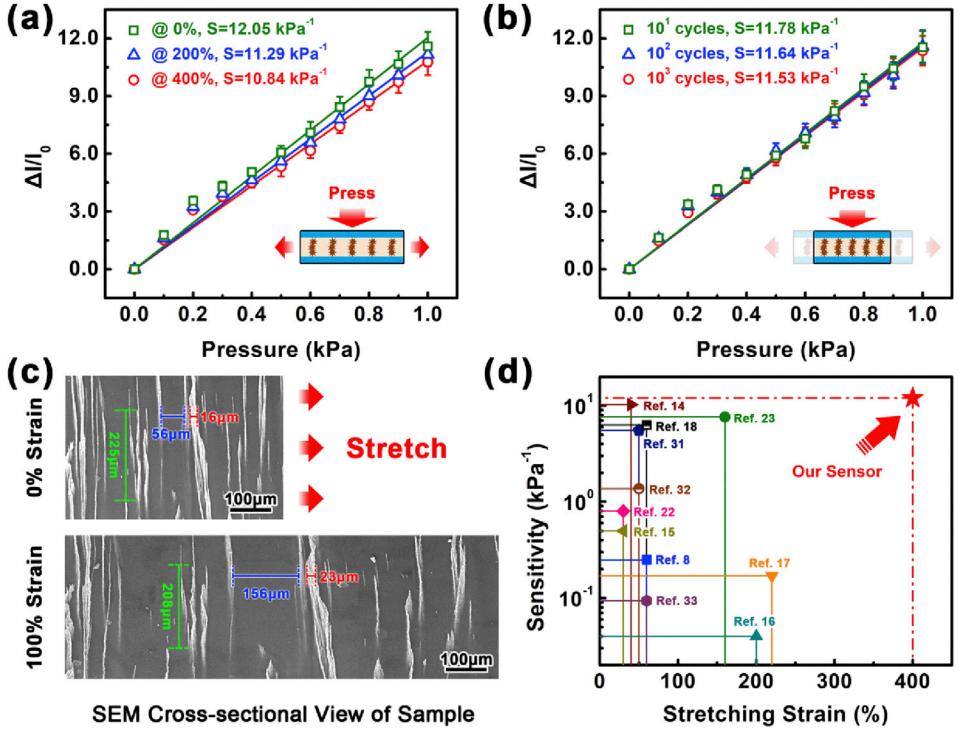

Fig. 2. Relative electrical response of our STS as a function of the loading pressure (a) at different stretching strain and (b) after several stretching cycles. (c) SEM cross-sectional view images of US-CMNPs@PU composite at 0% and 100% stretching strain. (d) Comparison of current work and previously reported STS performance: pressure sensitivity and dynamic stability. STS, stretchable tactile sensor; US-CMPNs, urchin-shaped conductive magnetic nanoparticles; PU, polyurethane.

the performance of our STS was investigated (Fig. 2b). The sensitivity of pressure is unchanged after repeated stretching cycles at 400% stretching strain ($S = 11.78\ kPa^{-1}$ @ 10 cycles, $S = 11.64\ kPa^{-1}$ @ 100 cycles, and $S = 11.53\ kPa^{-1}$ @ 1,000 cycles). There is a slight attenuation of the electrical response to pressure under increased stretching strain or cycling. For example, the attenuation of sensitivity is reduced slightly to 10.04% from the original state, when the STS is stretched to 400% strain (Fig. 2a). Similarly a decrease of sensitivity to 4.32% occurs after 1,000 stretching cycles (Fig. 2b). This attenuation can be attributed to the effect of Poisson's ratio in the composite. When the US-CMNPs@PU piezoresistive composite is stretched, it undergoes a small contraction of 7.56% in the vertical direction from 225 μm to 208 μm (green line, Fig. 2c), which can affect the piezoresistive response. More importantly, we have found that the microprotrusion hardens after stretching, in accordance with the mechanics simulation because of strain hardening by the effect of Poisson's ratio. It will weaken the pressure sensitivity of sensor. The vertically aligned columns of US-CMNPs are also slightly widened by stretching, which can also result in the attenuation of the piezoresistive effect. The change in the width of the columns can be better seen from the red line (Fig. 2c), which changes from 16 μm to 23 μm (43.76% deformation strain) at 100% stretching strain. But this change is small compared with the change in distance between two columns, i.e. the pure matrix region (blue line, Fig. 2c). Stretching strain in the pure matrix region is as high as 178.57%, widening from 56 μm to 156 μm. Thus, STS engineered with different elastic modulus regions enable strain accommodation during high stretching load and also during repeated stretching cycles. The pressure sensitivity of our STS is highly dynamically stable up to 400% stretching strain, which means that the sensor displays a good non-interference capability suitable for practical applications.

In Fig. 2d, our STS based on US-CMNPs@PU piezoresistive composite is compared with previously reported STSs to highlight the performance of our sensor in terms of pressure sensitivity and non-interference of stretching strain. Our STS is among the top performers in reported pressure sensitivity and displays an unprecedented high dynamic stability under stretching strain. Its non-interference capability of stretching strain is 2–10 times higher than that of others [8,14–18,22,23,31–33]. The non-interference capability of reported STSs is mostly between 30% and 60% stretching strain, and a few STSs can reach 200% stretching strain (Fig. 2d). This confirms that our bottom-up strategy is an effective approach to fabricate piezoresistive composite STSs with high performance via regulation of the elastic modulus in different functional regions to realize strain accommodation at large stretching strain.

In addition, the other key pressure sensing parameters of our STS are also excellent, as shown in Fig. 3. From Fig. 3a, it can be found that the electrical response curves of our sensor coincide well under loading and unloading of pressure. The hysteresis coefficient (H) of the STS based on US-CMNPs@PU composite is a low value of 5.25% (Fig. 3a), which is calculated in accordance with the following equation:

$$H = \frac{A_1 - A_2}{A_1} \times 100\% \quad (2)$$

where A_1 is the area among the loading curve, the line of $\Delta I/I_0 = 0$, and line of Pressure = 1 kPa. Although A_2 is the area among unloading curve, the line of $\Delta I/I_0 = 0$, and line of pressure = 50 kPa. Fig. 3bshow the results of the sensor tested by light weights, such as soft foam (106 mg), dried flower (51 mg), and a spider (22 mg). Even at a stretching strain of 400%, the sensor can perceive these light weights well, retaining the minimum detection limit. From Fig. 3c–d, it can be found that our sensor has a low response/recovery time (<50 ms), no matter at original state or stretched state. Importantly, our sensor has excellent mechanical durability, which can be seen in Fig. 3e, where the sensing response was tested over 10,000 stretching cycles, and an additional 10,000 pressure loadings. Although there is a fluctuation in sensing response ($\Delta I/I_0 = 0.008$) during the repeated mechanical loading (inset (1)–(2) of Fig. 3e), the change is negligible compared to the sensitivity value of the pressure response (inset (3)–(4) of Fig. 3e). The mechanical durability of sensor is derived from the selected PU matrix, which possesses a NPR functional group in the hard segments. Compared with a traditional PU composite that introduces a planar benzene ring in the hard segments , our composite sample (US-CMNPs@NPR-PU) has high recovery and fatigue resistance after stress relaxation test (400% stretching strain for 20 h). This high performance can be attributed to the NPR structure, which absorbs and releases strain energy through a chair-boat conformational transition to protect the polymer network [51–53]. This phenomenon was observed from small angle X-ray scattering.

The more detailed comparison of tactile sensors based on piezoresistive composites is listed in Table 1, including their pressure sensitivity, response time, detection limit, cycling times, and stretchability values. It can be observed that the various performance of our sensor is at the forefront of that of STSs. Compared with common flexible tactile sensors, the pressure sensitivity and detection limit of our sensor need to be further improved (>50 kPa^{-1}, <10 ms), which is an important research and development for STS in future. We think it can be solved by preparing new function fillers, such as hollow urchin-shaped fillers formed by the nanofibers.

2.3. Prototype electronic systems

To show the advantage of our STS based on US-CMNPs@PU piezoresistive composite, we investigated its performance as a front-end sensor for WED, HMI, and E-skin. In the fabricated WED, as shown in Fig. 4a, the STS is worn on the knee. The signal acquisition circuit diagram. When the sensor is touched by a finger five times, there are five corresponding large electrical signal peaks ($\Delta I/I_0$ = 12.24–14.72). The slight magnitude changes can be attributed to the human error in replicating the touches. When the wearer repeatedly squats, the signal of the sensor is stable. When held in a squat position, there are still five large electrical signal peaks when a finger touches the sensor 5 times. . This shows that WED based on our sensor overcome the shortcomings of conventional devices which are generally incapable of sensitively perceiving the applied pressure under practical application conditions. For example, a football or basketball player can wear our sensor to detect the damage caused by collisions. The STS was also used as an HMI on the surface of air balloon to control inflation from the gas cylinder. . When the sensor is not activated, the air valve controller present between the balloon and the cylinder is open to fill gas into a balloon, resulting in expansion. When the sensor is activated by touching, the air valve controller receives a feedback signal to close and inflation ceases. Photographs and response data are shown in Fig. 4b–c. When the balloon is expanded to more than twice its original volume (① vs. ③), the sensor control is still good (② vs. ④), with no reduction in performance with repetition. This performance is due to excellent non-interference ability under stretching strain and cycling of our sensor. The sensor may also be applied as a receptor for a soft robot to perceive the immediate physical environment and avoid obstacles for planing the robot's motion.

Finally, we demonstrate the performance of an STS array based on US-CMNPs@PU composite with 6 × 6 pixels to be used as a

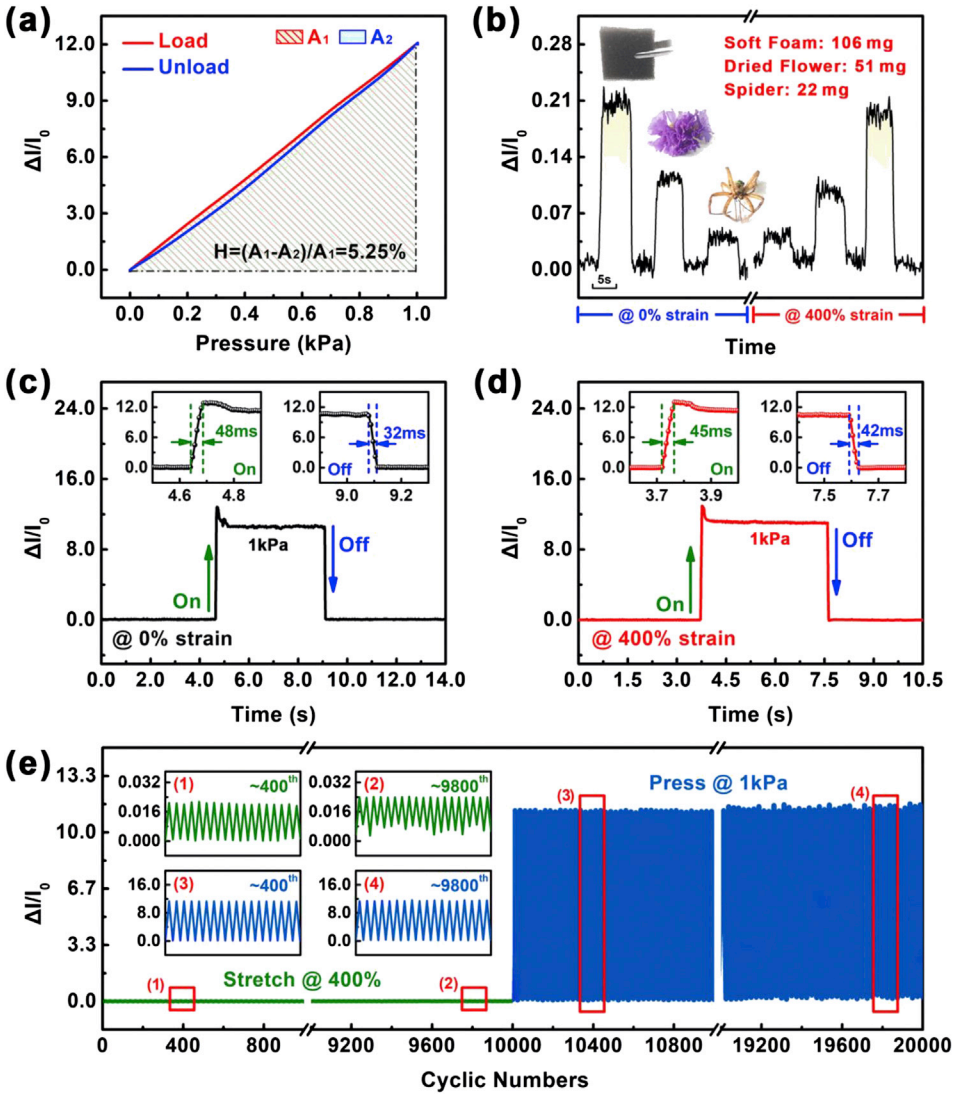

Fig. 3. (a) Relative electrical response of our STS as a function of loading pressure and the unloading pressure. (b) Relative electrical response of our STS for several light objects under stretching strain of 0%, and 400%. Relative electrical response of our STS to rapidly loaded and unloaded pressure under stretching strain of (c) 0% and (d) 400%. (e) Relative electrical response of our STS during repeated stretching for 10,000 times, and followed by repeated pressure sensing for 10,000 times. STS, stretchable tactile sensor.

Table 1
The more detailed comparison of tactile sensors based on piezoresistive composites.

Reference	Sensitivity (kPa^{-1})	Response time (ms)	Detection limit	Cycling times	Stretchability
Our	12.05	40	22 mg	10,000	400%
14	4.88	150	93 mg	800	40%
15	0.5	62.5	131.4 Pa	2,000	30%
18	6.3	50	10 mg	5,000	60%
31	5.54	25	17 mg	10,000	50%
13	133.1	47	8 mg	8,000	–
30	121	16	0.015 Pa	2,000	–
40	56.36	300	4 mg	25,000	–
25	31.6	100	0.6 Pa	15,000	–
21	19.8	16.7	0.6 Pa	35,000	–
19	17.2	90	300 Pa	300	–
29	15.1	44	0.2 Pa	100	–
24	10	20	400 mg	1,000	–
46	8.5	35	10.2 mg	10,000	–
27	2.46	30	100 Pa	200	–
20	0.71	82.6	0.02 N	500	–
28	0.122	9	0.568 Pa	1,000	–
13	133.1	47	8 mg	8,000	–

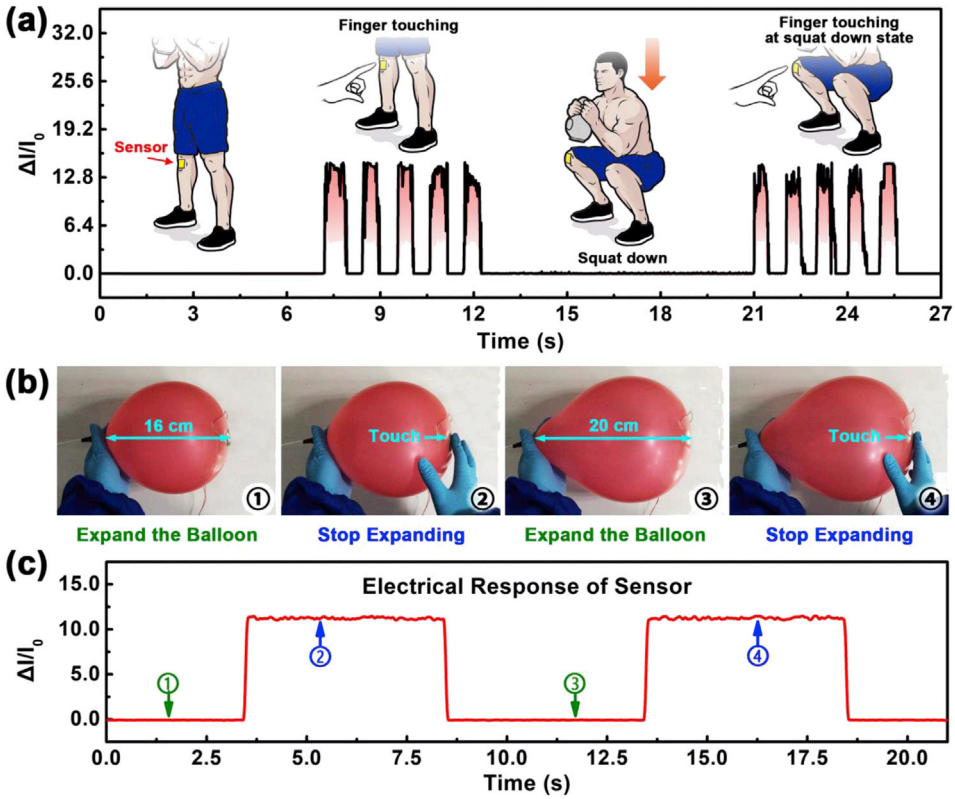

Fig. 4. (a) Relative electrical response of WED based on our STS to the pressure sensing of finger touch during squatting up and down. Insets show the schematic illustrations of sensing state corresponding to different electrical responses that includes no touching at upright state, touching at upright state, no touching at squat state, and touching at squat state. (b) Optical photos and (c) relative electrical response of HMI based on our STS during the control process of expanding the balloon via touching the STS. STS, stretchable tactile sensor; WED, wearable electrical device.

stretchable E-skin. The schematic structure and sample picture of this array are shown in Fig. 5a–b. The LM-based elastic electrode layer is prepared by screen printing [54,55], and the area of each pixel is 25 mm^2. Every pixel of the array is equipped with a high-pressure sensitivity STS. To obtain the response data of each pixel in real-time, we developed a back-end acquisition system for the E-skin. This stretchable E-skin is successfully demonstrated to identify the shape of different objects accurately, in both original and stretched states, equivalent to relaxed and tightened states of human skin (Fig. 5c). The objects placed on the sensor array were a round button cell battery and a cylindrical dry cell battery. From an analysis of the signal response maps, the identified shape area of the button cell at the stretched state is 88.75%–94.81% of that of the original state. To improve shape recognition using the stretchable E-skin, a high-resolution STS array can be developed by reducing the size and spacing of the pixels. The pixel area of high-resolution sensor arrays should be less than 1 mm^2, which is the next production challenge for stretchable E-skin based on STS arrays.

3. Conclusion

In this study, we report an STS based on an US-CMNPs@PU piezoresistive composite, wherein the US-CMNPs are vertically aligned columns and horizontally isolated in the PU matrix. The composite has different elastic modulus in the corresponding functional regions for pressure sensing (E = 59.1 MPa) and releasing the stretching strain (E = 2.4 MPa) to realize strain accommodation under large stretching deformation. The resulting STS exhibits high-pressure sensitivity (12.05 kPa^{-1}) and an excellent dynamic stability ($\Delta S/S_0$ <10.5% @ 400% strain). Its performance is far superior to that of previously reported STS. In addition, our STS displays good performance in other key pressure-sensing parameter, unstretched or stretched, such as hysteresis coefficient, minimum detection limit, response/recovery time, and mechanical durability. This work also demonstrates the feasibility of our sensor as a stretchable front-end sensor of several important application systems, such as WEDs, HMI, and E-skin. These results reveal that the bottom-up strategy of elastic modulus regulation is an easy-operative approach to separate sensing from multiple stimulus. The US-CMNPs@PU composite STS, and the developed fabrication method, will promote the development of new electronic systems with multiple functions and high performance. Based on this research, we will improve the detection range of sensor and then further develop a E-skin with high resolution and large area to rival real skin.

4. Experimental Section

4.1. Synthesis of US-CMNPs

The US-CMNPs were synthesized by the seed growth of chemical reduction using the Ag-Ni nanoparticles as seed, L-Dopa (99%, Shanghai Aladdin Co., Ltd.) as the reduction agent, and $HAuCl_4 \cdot 4H_2O$ (>47.8%, Sinopharm Chemical Reagent Co., Ltd.) as the source of Au^{3+}. The Ag-Ni nanoparticles was prepared by dispersing the Ni nanoparticles (100 nm, Suzhou Canfuo Nanotechnology Co.,Ltd) in diluted $AgCl_3$ solution (2%, Sinopharm Chemical Reagent Co., Ltd.) and diluted ammonia (2%, Sinopharm

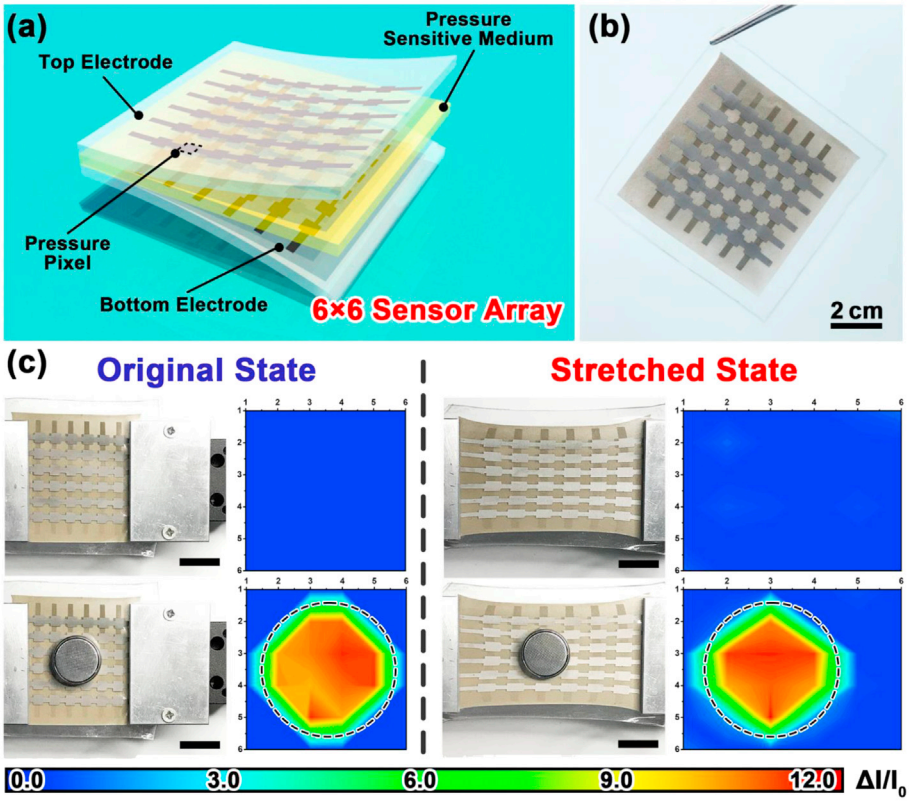

Fig. 5. (a) Schematic illustration of E-skin based on our STS array with 6 × 6 pixels. (b) Optical photo of STS array sample. (c) Optical photos of STS array loaded by different objects at original/stretched states, and corresponding mapping of the electrical changes. STS, stretchable tactile sensor; E-skin, electronic skin.

Chemical Reagent Co., Ltd.) is dropped stepwise. First, $HAuCl_4$ aqueous solution (10 mM) was mixed with DI water in the ratio of 1:2 by volume. Then, the diluted solution was put into an oil bath at constant cold temperature. After 15 min, Ag-Ni nanoparticles with equal mass of $HAuCl_4$ aqueous solution were fed into the system, followed by the addition of L-Dopa aqueous solution (10 mM) with an equal volume of $HAuCl_4$ aqueous solution to react with it. In this process, the system should be gas stirred. After several minutes, the nanoparticles in the mixture solution were separated by centrifugation (YZB/wanhe0006-2009, Anhui USTC Zonkia Scientific Instruments Co., Ltd.). Finally, the particles were washed to obtain US-CMNP because the bath temperature has a great influence on the micro morphology of particles. The optimum bath temperature used is 10 °C to obtain US-CMNPs.

4.2. Preparation of US-CMNPs@PU composite and STS

First, US-CMNPs were mixed with PU solution (10 wt%) using anhydrous dimethylformamide (DMF, 99.5%, Shanghai Aladdin Co., Ltd.) as solvent in the mass ratio of 1:2 by mechanical stirring. . Then, the mixture was poured into a teflon mould to stand for 1 h. Then, the mould fitted with the mixture was put in a self-built device with a vertical magnetic field. The magnetic field intensity can be adjusted by the distance of two permanent magnets (NdFeB, Shanghai Haoyang Electromagnetic Machinery Co., Ltd.), which is in-built in the device. Afterward, the obtained product was dried in a vacuum oven (DZF-6123, Shanghai Yiheng Scientific Instruments Co., Ltd.) at 60 °C under vacuum. US-CMNPs@NPR-PU composite was obtained after drying it for 24 h. Finally, US-CMNPs@NPR-PU composite was sandwiched between top and bottom elastic electrodes based on LMs to prepare the final stage of STS preparation. The preparation process of LMs-based elastic electrode and also detailed in our previous report by Yu et al. [44], Ying et al.[54], and Zhang et al. [55].

4.3. Characterization of microstruture

The microstructures of samples were characterized by the field-emission scanning electron microscopy (Sirion 200, FEI; Verios G4 UC, Thermo scientific) and the laser scanning confocal microscope (LSM700, Zeiss).

4.4. Measurements of Mechanical/Electrical Property of US-CMNPs@PU composite and the sensing property of STS

The mechanical property of composite was measured by the universal material testing machine (Instron 5943). The stretching speed was 30–90 mm/min. The elastic modulus of different functional regions was tested by the nanoindentation (MTS, G200). The displacement of pressure loading was 1,000 nm. The stretching strain color map was measured from GOM Optical Technology (Shanghai) Co., Ltd. by ARAMS, when the sample was stretched. The sensing property of STS was measured by the DC current source, the nanovoltmeter, and the oscilloscope (710110/DLM2024, Yokogawa). The electrical property of composite and the sensing property of STS were measured by the DC current source (Keithley 6221) and the nanovoltmeter (Agilent 34420A). In these experiments, the pressure force and stretching strain were applied by the Instron 5943 and the universal material testing machine and linear stretching module of stepping motor (Chengdu Fuyu technology Co., Ltd), respectively.

4.5. Synthesis of NPR-PU

In the 99.999% Ar glove box, 20 g dry poly (tetramethylene glycol) (PTMG, 2,000 g/mol, Shanghai Aladdin Co., Ltd.) was poured into a dry three-neck reactor equipped with a mechanical stirrer, followed by the addition of 0.25 g dibutyltin dilaurate (95%, Shanghai Aladdin Co., Ltd.), 50 ml DMF and 8.9 ml isophorone diisocyanate (IPDI, 99%, Shanghai Aladdin Co., Ltd.). Then the reactor was sealed by rubber septum and kept at 65 °C using oil bath for 1 h prepolymerization. After that, a desired amount of 5.95 g hydroquinone bis(2-hydroxyethyl)ether (HQEE, 95%, Shanghai Aladdin Co., Ltd.) was dissolved in DMF and injected drop wise into the sealed reactor for chain extension. The final concentration was adjusted to 30 wt% in this system by adding a desired amount of DMF. Then the whole system was heated at 80 °C for another 4 h to obtain the complete polymerization. Finally, the polymer was precipitated into the excess distilled water and washed several times, followed by the vacuum drying at 60 °C for 24 h to constant weight.

4.6. Synthesis of PR-PU

The synthesis method was similar to that of NPR-PU but using 4,4′-methylenebis (phenyl isocyanate) (98%, Shanghai Aladdin Co., Ltd.) instead of IPDI.

4.7. Characterization of NPR-PU

SAXS experiments were carried out on the beamline BL16B1 in the Shanghai Synchrotron Radiation Facility with a 0.124 nm X-ray wavelength and the obtained data was analyzed by Fit2D software quantitatively. ^{1}H-Nuclear Magnetic Resonance (NMR) spectra was carried out on AVANCE III (400 MHz) at room temperature with tetramethylsilane as an internal standard, and the sample concentrations were in the range of 1–10 wt%. Attenuated total reflectance-Fourier Transform Infrared Spectroscopy (FTIR) absorption spectra were measured on an iD5 ZnSe ATR (Cary660, Agilent).

Declaration of Competing Interest

The authors declare no competing interests.

Acknowledgments

The authors acknowledge the financial support from the China International Cooperation Project (2016YFE0126700), National Natural Science Foundation of China (61774161, 51525103, 51931011, and 51773218), Public Welfare Technical Applied Research Project of Zhejiang Province (2017C31100), Natural Science Foundation of Zhejiang Province (LQ19E030005), Ningbo Scientific and Technological Innovation 2025 Major Project (2018B10057), and Natural Science Foundation of Ningbo (2018A610109).

References

[1] P. Li, Y. Wen, An arbitrarily distributed tactile piezoelectric sensor array, Sens. Actuators, A 65 (1998) 141–146.
[2] O. Müller, W.J. Park, M.G. Wiedemann, F. Martini, Three-dimensional measurements of the pressure distribution in artificial joints with a capacitive sensor array, J. Biomech. 37 (2004) 1623–1625.
[3] M. Shimojo, A. Namiki, M. Ishikawa, R. Makino, K. Mabuchi, A tactile sensor sheet using pressure conductive rubber with electrical-wires stitched method, IEEE Sensor. J. 4 (2004) 589–596.
[4] T. Someya, T. Sekitani, S. Iba, Y. Kato, H. Kawaguchi, T. Sakurai, A large-area, flexible pressure sensor matrix with organic field-effect transistors for artificial skin applications, Proc. Natl. Acad. Sci. U.S.A. 101 (2014) 9966–9970.
[5] N. Marian, A. Drimus, A. Bilberg, Development of a tactile sensor array, Solid State Phenom. 166–167 (2010) 277–284.
[6] Q.-J. Sun, J. Zhuang, S. Venkatesh, Y. Zhou, S.-T. Han, W. Wu, K.-W. Kong, W.-J. Li, X. Chen, R.K.Y. Li, V.A.L. Roy, Highly sensitive and ultrastable skin sensors for biopressure and bioforce measurements based on hierarchical microstructures, ACS Appl. Mater. Interfaces 10 (2018) 4086–4094.
[7] J. Kim, M. Lee, H.J. Shim, R. Ghaffari, H.R. Cho, D. Son, Y.H. Jung, M. Soh, C. Choi, S. Jung, K. Chu, D. Jeon, S. Lee, J.H. Kim, S.H. Choi, T. Hyeon, D. Kim, Stretchable silicon nanoribbon electronics for skin prosthesis, Nat. Commun. 5 (2014) 5747.
[8] T.Y. Choi, B.-U. Hwang, B.-Y. Kim, T.Q. Trung, Y.H. Nam, D.-N. Kim, K. Eom, N.-E. Lee, Stretchable, transparent, and stretch-unresponsive capacitive touch sensor array with selectively patterned silver nanowires/reduced graphene oxide electrodes, ACS Appl. Mater. Interfaces 9 (2017) 18022–18030.
[9] S. Wang, J. Xu, W. Wang, G.-J.N. Wang, R. Rastak, F. Molina-Lopez, J.W. Chung, S. Niu, V.R. Feig, J. Lopez, T. Lei, S.-K. Kwon, Y. Kim, A.M. Foudeh, A. Ehrlich, A. Gasperini, Y. Yun, B. Murmann, J.B.-H. Tok, Z. Bao, Skin electronics from scalable fabrication of an intrinsically stretchable transistor array, Nature 555 (2018) 83–88.
[10] C.F. Wang, C.H. Wang, Z.L. Huang, S. Xu, Materials and structures toward soft electronics, Adv. Mater. 30 (2018) 1801368.
[11] M.L. Hammock, A. Chortos, B.C.-K. Tee, J.B.-H. Tok, Z. Bao, 25th anniversary article: the evolution of electronic skin (E-Skin): a brief history, design considerations, and recent progress, Adv. Mater. 25 (2013) 5997–6038.
[12] Y. Wan, Y. Wang, C.F. Guo, Recent progresses on flexible tactile sensors, Mater. Today Phys. 1 (2017) 61–73.
[13] L. Pan, A. Chortos, G. Yu, Y. Wang, S. Isaacson, R. Allen, Y. Shi, R. Dauskardt, Z. Bao, An ultra-sensitive resistive pressure sensor based on hollow-sphere microstructure induced elasticity in conducting polymer film, Nat. Commun. 5 (2014) 3002.
[14] C.-L. Choong, M.-B. Shim, B.-S. Lee, S. Jeon, D.-S. Ko, T.-H. Kang, J. Bae, S.H. Lee, K.-E. Byun, J. Im, Y.J. Jeong, C.E. Park, J.-J. Park, U.-i. Chung, Highly stretchable resistive pressure sensors using a conductive elastomeric composite on a micropyramid array, Adv. Mater. 26 (2014) 3451–3458.
[15] E. Roh, H.-B. Lee, D.-I. Kim, N.-E. Lee, A solution-processable, omnidirectionally stretchable, and high-pressure-sensitive piezoresistive device, Adv. Mater. 29 (2017) 1703004.
[16] B. Li, Y. Gao, A. Fontecchio, Y. Visell, Soft capacitive tactile sensing arrays fabricated via direct filament casting, Smart Mater. Struct. 25 (2016): 075009.
[17] S. Biswas, J. Reiprich, J. Pezoldt, T. Stauden, H.O. Jacobs, Metamorphic stretchable touchpad, Adv. Mater. Technol. 4 (2019) 1800446.
[18] J.C. Yang, J.-O. Kim, J. Oh, S.Y. Kwon, J.Y. Sim, D.W. Kim, H.B. Choi, S. Park, Microstructured porous pyramid-based ultrahigh sensitive pressure sensor insensitive to strain and temperature, ACS Appl. Mater. Interfaces 11 (2019) 19472–19480.
[19] L.-Q. Tao, K.-N. Zhang, H. Tian, Y. Liu, D.-Y. Wang, Y.-Q. Chen, Y. Yang, T.-L. Ren, Graphene-paper pressure sensor for detecting human motions, ACS Nano 11 (2017) 8790–8795.
[20] J. Wang, M. Tenjimbayashi, Y. Tokura, J.-Y. Park, K. Kawase, J. Li, S. Shiratori, Bionic fish-scale surface structures fabricated via air/water interface for flexible and ultrasensitive pressure sensors, ACS Appl. Mater. Interfaces 10 (2018) 30689–30697.
[21] M.Q. Jian, K.L. Xia, Q. Wang, Z. Yin, H.M. Wang, C.Y. Wang, H.H. Xie, M.C. Zhang, Y.Y. Zhang, Flexible and highly sensitive pressure sensors based on bionic hierarchical structures,, Adv. Funct. Mater. 27 (2017) 1606066.
[22] S. Lim, D. Son, J. Kim, Y.B. Lee, J.K. Song, S. Choi, D.J. Lee, J.H. Kim, M. Lee, T. Hyeon, D.H. Kim, Transparent and stretchable interactive human machine interface based on patterned graphene heterostructures, Adv. Funct. Mater. 25 (2015) 375–383.
[23] T. Bu, T. Xiao, Z. Yang, G. Liu, X. Fu, J. Nie, T. Guo, Y. Pang, J. Zhao, F. Xi, C. Zhang, Z.L. Wang, Stretchable triboelectric-photonic smart Skin for tactile and gesture sensing, Adv. Mater. 30 (2018) 1800066.
[24] S. Lee, A. Reuveny, J. Reeder, S. Lee, H. Jin, Q. Liu, T. Yokota, T. Sekitani, T. Isoyama, Y. Abe, Z. Suo, T. Someya, A transparent bending-insensitive pressure sensor, Nat. Nanotechnol. 11 (2016) 472–478.
[25] Z. Lou, S. Chen, L.L. Wang, R.L. Shi, L. Li, K. Jiang, D. Chen, G.Z. Shen, Ultrasensitive and ultraflexible e-skins with dual functionalities for wearable electronics, Nano Energy 38 (2017) 28–35.
[26] A. Chortos, J. Liu, Z. Bao, Pursuing prosthetic electronic skin, Nat. Mater. 15 (2016) 937–950.
[27] D. Lee, H. Lee, Y. Jeong, Y. Ahn, G. Nam, Y. Lee, Highly sensitive, transparent, and durable pressure sensors based on sea-urchin shaped metal nanoparticles, Adv. Mater. 28 (2016) 9364–9369.
[28] Y. Wu, H. Liu, S. Chen, X. Dong, P. Wang, S. Liu, Y. Lin, Y. Wei, L. Liu, Channel crack-designed gold@PU sponge for highly elastic piezoresistive sensor with excellent detectability, ACS Appl. Mater. Interfaces 9 (2017) 20098–20105.
[29] J. Park, Y. Lee, J. Hong, M. Ha, Y.-D. Jung, H. Lim, S.Y. Kim, H. Ko, Giant tunneling piezoresistance of composite elastomers with interlocked microdome arrays for ultrasensitive and multimodal electronic skins, ACS Nano 8 (2014) 4689–4697.
[30] B. Yin, X. Liu, H. Gao, T. Fu, J. Yao, Bioinspired and bristled microparticles for ultrasensitive pressure and strain sensors, Nat. Commun. 9 (2018) 5161.

[31] Z. Wang, X. Guan, H. Huang, H. Wang, W. Lin, Z. Peng, Full 3D printing of stretchable piezoresistive sensor with hierarchical porosity and multimodulus architecture, Adv. Funct. Mater. 29 (2019) 1807569.
[32] T.-H. Chang, Y. Tian, C. Li, X. Gu, K. Li, H. Yang, P. Sanghani, C.M. Lim, H. Ren, P.-Y. Chen, Stretchable graphene pressure sensors with shar-pei-like hierarchical wrinkles for collision-aware surgical robotics, ACS Appl. Mater. Interfaces 11 (2019) 10226–10236.
[33] J. Zhao, C. Zhang, D. Zou, X. Liu, L. Cai, X. Li, M. Shi, A structured design for highly stretchable electronic skin, Adv. Mater. Technol. 4 (2019) 1900492.
[34] J. Park, Y. Lee, J. Hong, Y. Lee, M. Ha, Y. Jung, H. Lim, S.Y. Kim, H. Ko, Tactile-direction-sensitive and stretchable electronic skins based on human-skin-inspired interlocked microstructures, ACS Nano 8 (2014) 12020–12029.
[35] S. Jung, J.H. Kim, J. Kim, S. Choi, J. Lee, I. Park, T. Hyeon, D.-H. Kim, Reverse-micelle-induced porous pressure-sensitive rubber for wearable human-machine Interfaces, Adv. Mater. 26 (2014) 4825–4830.
[36] S. Yao, Y. Zhu, Nanomaterial-enabled stretchable conductors: strategies, materials and devices, Adv. Mater. 27 (2015) 1480–1511.
[37] J.C. Yang, J. Mun, S.Y. Kwon, S. Park, Z. Bao, S. Park, Electronic skin: recent progress and future prospects for skin-attachable devices for health monitoring, robotics, and prosthetics, Adv. Mater. 31 (2019) 1904765.
[38] S. Chen, Y.J. Song, D.Y. Ding, Z. Ling, F. Xu, Flexible and anisotropic strain sensor based on carbonized crepe paper with aligned cellulose fibers, Adv. Funct. Mater. 28 (2018) 1802547.
[39] J.-H. Lee, J. Kim, D. Liu, F. Guo, X. Shen, Q.B. Zheng, S. Jeon, J.-K. Kim, Highly aligned, anisotropic carbon nanofiber films for multidirectional strain sensors with exceptional selectivity, Adv. Funct. Mater. 29 (2019) 1901623.
[40] L.L. Wang, J.A. Jackman, E.L. Tan, J.H. Park, M.G. Potroz, E.T. Hwang, N.J. Cho, High-performance, flexible electronic skin sensor incorporating natural microcapsule actuators, Nano Energy 36 (2017) 38–45.
[41] L. Chen, B. Su, L. Jiang, Recent advances in one-dimensional assembly of nanoparticles, Chem. Soc. Rev. 48 (2019) 8–21.
[42] Z. Liu, Z.B. Yang, B. Peng, C. Cao, C. Zhang, H.J. You, Q.H. Xiong, Z.Y. Li, J.X. Fang, Highly sensitive, uniform, and reproducible surface-enhanced Raman spectroscopy from hollow Au-Ag alloy nanourchins, Adv. Mater. 26 (2014) 2431–2439.
[43] J. Xie, J.Y. Lee, D.I.C. Wang, Seedless, surfactantless, high-yield synthesis of branched gold nanocrystals in HEPES buffer solution, Chem. Mater. 19 (2007) 2823–2830.
[44] Z. Yu, J. Shang, X. Niu, Y. Liu, G. Liu, P. Dhanapal, Y. Zheng, H. Yang, Y. Wu, Y. Zhou, Y. Wang, D. Tang, R.-W. Li, A composite elastic conductor with high dynamic stability based on 3D-calabash bunch conductive network structure for wearable devices, Adv. Electron. Mater. 4 (2018) 1800137.
[45] J. Shi, L. Wang, Z. Dai, L. Zhao, M. Du, H. Li, Y. Fang, Multiscale hierarchical design of a flexible piezoresistive pressure sensor with high sensitivity and wide linearity range, Small 14 (2018) 1800819.
[46] G.Y. Bae, S.W. Pak, D. Kim, G. Lee, D.H. Kim, Y. Chung, K. Cho, Linearly and highly pressure-densitive electronic skin based on a bioinspired hierarchical structural array, Adv. Mater. 28 (2016) 5300–5306.
[47] A.d. Santos, N. Pinela, P. Alves, R. Santos, E. Fortunato, R. Martins, H. Águas, R. Igreja, Piezoresistive e-skin sensors produced with laser engraved molds, Adv. Electron. Mater. 4 (2018) 1800182.
[48] Y. Pang, K. Zhang, Z. Yang, S. Jiang, Z. Ju, Y. Li, X. Wang, D. Wang, M. Jian, Y. Zhang, R. Liang, H. Tian, Y. Yang, T.-L. Ren, Epidermis microstructure inspired graphene pressure sensor with random distributed spinosum for high sensitivity and large linearity, ACS Nano 12 (2018) 2346–2354.
[49] Y. Shu, H. Tian, Y. Yang, C. Li, Y. Cui, W. Mi, Y. Li, Z. Wang, N. Deng, B. Peng, Surface-modified piezoresistive nanocomposite flexible pressure sensors with high sensitivity and wide linearity, Nanoscale 7 (2015) 8636–8644.
[50] K. Kim, M. Jung, B. Kim, J. Kim, K. Shin, O.-S. Kwon, S. Jeon, Low-voltage, high-sensitivity and high-reliability bimodal sensor array with fully inkjet-printed flexible conducting electrode for low power consumption electronic skin, Nano Energy 41 (2017) 301–307.
[51] L. Zhang, S.S. Shams, Y. Wei, X. Liu, S. Ma, R. Zhang, J. Zhu, Origin of highly recoverable shape memory polyurethanes (SMPUs) with non-planar ring structures: a single molecule force spectroscopy investigation, J. Mater. Chem. 2 (2014) 20010–20016.
[52] P.E. Marszalek, A.F. Oberhauser, Y.-P. Pang, J.M. Fernandez, Polysaccharide elasticity governed by chair-boat transitions of the glucopyranose ring, Nature 396 (1998) 661–664.
[53] W. Xu, R. Zhang, W. Liu, J. Zhu, X. Dong, H. Guo, G.-H. Hu, A multiscale investigation on the mechanism of shape recovery for IPDI to PPDI hard segment substitution in polyurethane, Macromolecules 49 (2016) 5931–5944.
[54] W.B. Ying, Z. Yu, D.H. Kim, K.J. Lee, H. Hu, Y.W. Liu, Z.Y. Kong, K. Wang, J. Shang, R.Y. Zhang, J. Zhu, R.-W. Li, Water proof, highly tough and fast self-healing polyurethane for durable electronic skin, ACS Appl. Mater. Interfaces 12 (2020) 11072–11083.
[55] Y.-N. Zheng, Z. Yu, G.Y. Mao, Y.Y. Li, D. Pravarthana, W. Asghar, Y.W. Liu, S.X. Qu, J. Shang, R.-W. Li, A wearable capacitive sensor based on ring/disc-shaped electrode and porous dielectric for non-contact healthcare monitoring, Global Chall. 4 (2020) 1900079.